# Analysis of Detached-Eddy Simulation for the Flow around a Circular Cylinder with Reference to PIV Data

**Charles MOCKETT**[1], **Rodolphe PERRIN**[1,2], **Thorsten REIMANN**[1], **Marianna BRAZA**[2] **and Frank THIELE**[1]

[1] *Institute of Fluid Mechanics and Engineering Acoustics (ISTA), TU-Berlin, Müller-Breslau-Str. 8, 10623 Berlin, Germany*
[2] *Institut de Mécanique des Fluides de Toulouse, Unité Mixte C.N.R.S.-I.N.P.T. 5502, Av. du Prof. Camille Soula, 31400 Toulouse, France*

**Abstract.** A detailed validation study is presented for the detached-eddy simulation (DES) of the flow around a circular cylinder at a high sub-critical Reynolds number. Direct comparability with unsteady experimental field data is ensured by the confined and clearly-defined geometry. The combination of DES with an appropriate low-dissipative hybrid numerical convection scheme and high temporal resolution delivers excellent agreement with the experiment for the time and phase-averaged fields and spectral content. A strong sensitivity of the solution to the numerical time step size has been identified, which is attributed to time-filtering effects damping the development of resolved turbulence in the early shear layer. Recommendations are made concerning a CFL-type criterion for the temporal resolution of DES, and the remaining small discrepancies are attributed to a still insufficient time resolution, giving a clear direction to future studies.

**Key words:** DES, time step sensitivity, bluff bodies, validation, PIV

## 1. Introduction

Detached-Eddy Simulation (DES) is a hybrid method for the treatment of massively separated, turbulent flows, which combines the use of URANS modelling in attached boundary layers, and LES in the separated turbulent regions. Since its conception [15], DES has been shown to demonstrate considerable improvements in predictive accuracy for bluff body flows, compared to pure URANS approaches [3, 7]. However, a detailed validation study including both time-averaged and unsteady wake field data and with direct comparability with experimental conditions is not known to the authors.

This study by contrast employs a test case with highly detailed experimental field data obtained by IMFT using time-resolved PIV techniques, for a circular cylinder in a confined domain allowing complete reproduction of the clearly-defined experimental geometry. As such, a deeper comparison and analysis of the performance and properties of DES can be conducted. The improvement of DES compared to URANS for bluff body flows is considered to be well-established, and accordingly only DES simulations will be considered here. An extensive study of DES for unconfined cylinders has been published by Travin et al. [16], in which the influence of grid resolution was investigated for a range of Reynolds numbers and constant time

step size (except for one low-$Re$ case). The findings of the present study will be compared to those of Travin et al. where relevant. Concerning the numerical time step size, it could be expected that DES would inherit a strong sensitivity to this from LES, and a variation of the time step size is therefore conducted to examine this issue. The investigation has been carried out within the framework of a bilateral cooperation between ISTA and IMFT, as well as the European DESider project.

## 2. Test case description and benchmark data

The test case under study is the flow around a circular cylinder of aspect ratio 4.8 spanning a square channel, which gives rise to a relatively high blockage coefficient of 0.208. A visual representation of the geometry is given in Fig. 1. The inflow velocity and cylinder diameter deliver a Reynolds number of $1.4 \times 10^5$, which has been shown in the experiment to correspond to the high sub-critical regime, where the cylinder boundary layer is laminar and the transition to turbulence can be assumed to take place immediately following separation. This regime is believed to occur at a lower Reynolds number than usually quoted in the literature because of a combination of the blockage effect and the free-stream turbulence intensity of 1.5% [8].

The experiments on this configuration [8, 9, 10] include very detailed measurements of the unsteady near-wake region using two-component (2C) as well as three-component (3C), stereoscopic PIV. High sampling rate measurements at 1000Hz have also been conducted offering true time resolution of the wake field (TRPIV). The PIV measurement planes are also depicted in Fig. 1, and are located at the spanwise centre plane normal to this axis.

All flow and geometrical quantities given will be normalised with respect to the inflow velocity $U_\infty = 15\text{m/s}$ and the cylinder diameter $D = 0.14\text{m}$.

## 3. Numerical method

The Navier–Stokes equations are discretised using a cell-centered finite volume method based on block-structured grids [18]. For the discretisation of the convective fluxes, both second order central and higher order upwind-biased limited schemes are available. The diffusive fluxes are approximated by a second order central-differencing scheme, and the pressure field is solved by the SIMPLE algorithm. A close coupling between pressure and convective velocity is achieved by the Rhie and Chow interpolation method [12].
In order to best address the inconsistency in the demands posed by RANS and LES on the numerical scheme for the convective fluxes, a hybrid scheme using a blending function, $\sigma$ has been proposed for DES by Travin et al. [17]. The $\sigma$ function assures an appropriate switch between upwind and central-based convection schemes in the RANS and LES zones respectively, and has been employed for the calculations presented within this study.

The DES is implemented on the basis of a compact explicit algebraic Reynolds stress (CEASM) RANS model [5], which employs the Lien and Leschziner $k - \varepsilon$

model [4] as a background model. The implementation includes a shield function to prevent the undesirable encroachment of the LES mode of DES into attached turbulent boundary layers (which can lead to a phenomenon known as "modelled stress depletion" or in extreme cases "grid-induced separation" [14, 6]). This shield function is a model-specific implementation following the methodology proposed by Menter and Kunz [6]. The RANS model length scale and the LES length scale are given by

$$L_{\mathrm{RANS}} = \frac{k^{\frac{3}{2}}}{\varepsilon}, \quad L_{\mathrm{LES}} = C_{\mathrm{DES}}\Delta_x, \tag{1}$$

respectively, where the LES spatial filter width $\Delta_x$ is formulated as the maximum of the grid cell dimesions in each index direction, i.e. $\Delta_x = \max[\Delta_i, \Delta_j, \Delta_k]$. More details on the model formulation can be found in Bunge et al. [1].

The reproduction of the experimental domain has been achieved using a block-structured grid of some 5 million points shown in Fig. 1, where 240 points are used around the cylinder circumference and 96 in the spanwise direction. The spanwise spacing is uniform along the central portion of the cylinder, with compression of the spacing towards each wall within a region of one diameter from each end. The spacing of the uniform section has been matched to that of the other grid directions in the "focus region" of the near wake to give roughly cubic cells here in accordance with DES grid guidelines [13]. The inflow plane, situated at the same location as the channel entrance in the experiment, is assumed to be far enough upstream of the cylinder ($7D$) for unsteadiness effects to be negligible. As such, a steady uniform velocity profile is applied here. A modification has been made to the $k$-equation, which suppresses the model's natural transition to ensure that the boundary layer on the cylinder remains laminar, and that transition occurs immediately following separation.

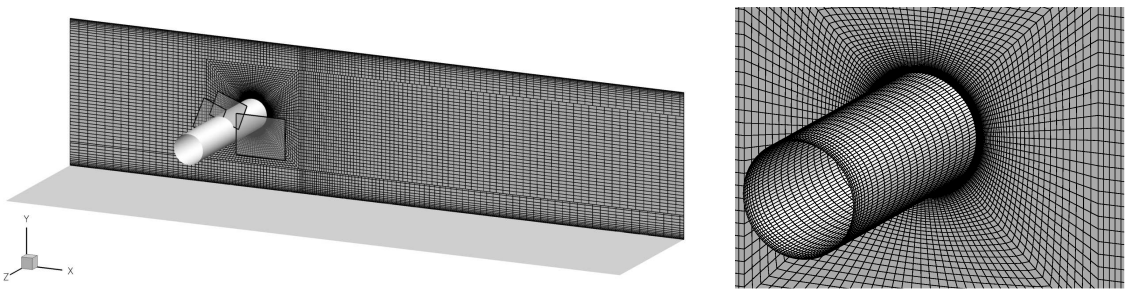


*Figure 1.* Test case configuration: Geometry, PIV planes and grid on $z$-slice located at wall *(left)*; zoom of near wake region with grid on cylinder and at $z$-slice through median plane *right*. Every second grid point omitted for clarity.

Two alternative time step sizes of $0.05D/U_\infty$ and $0.03D/U_\infty$ have been computed, whereby the coarser of the two matches that employed by Travin et al. [16]. For the coarse time step size, 3000 time steps have been collected for averaging, and 14000 for the fine time step, corresponding to physical times of $150D/U_\infty$ and $420D/U_\infty$ respectively.

## 4. Presentation and discussion of results

### 4.1. The instantaneous flow field

A visual impression of the flow physics and the structures resolved by the DES can be obtained from Fig. 2, which shows an instantaneous snapshot of the vortex cores obtained with the finer time step. Clearly-defined horseshoe vortices are evident at the cylinder/wall junctions, as are the breakup of the shear layer and the organisation of the chaotic turbulent eddies into a coherent vortex street pattern.

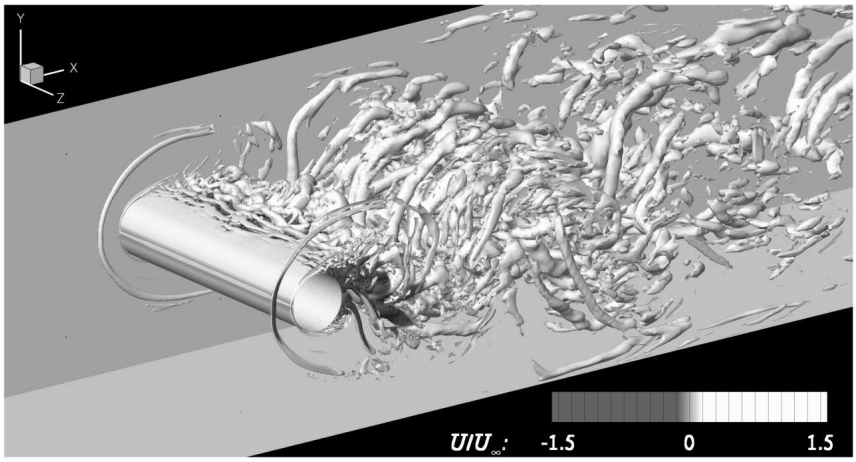


*Figure 2.* Instantaneous vortex core structures shown by isosurfaces of the $\lambda_2$ criterion shaded by streamwise velocity (dark shades denote reverse flow). DES with finer time step.

A two-dimensional snapshot of the wake region and the functionality of the DES is given by Fig. 3. Using the ratio of the RANS to LES length scales as an indicator, Fig. 3(b) shows the regions in which the alternative modes of the DES are in operation, whereby a value less or greater than unity corresponds to the RANS and LES modes respectively. The model can be seen to operate in LES-mode throughout the finely-resolved turbulent wake and in the outer irrotational flow region, and as RANS in the separated shear layers and outer edges of the turbulent wake. This kind of unsteady interface is typical of DES based on two-equation models, where the RANS length scale is derived locally from the model parameters (see Eq. 1) instead of the wall-normal distance as for one-equation models. This corresponds to a rough measure of the grid's capability to resolve the turbulent scales present at each point, reverting to RANS modelling when this is insufficient.

The distribution of the hybrid blending function, $\sigma$, is shown in Fig. 3(c). Values of $\sigma = 0$ and 1 correspond respectively to full central and upwind differencing of the convective fluxes, with flux blending applied at intermediate values. The distribution is seen to follow the turbulent wake region very well, with low-dissipative central differencing used there. The importance of such treatment for DES has been highlighted in precursor studies [1]. As the cylinder investigation of Travin et al. [16] predated the development of the hybrid convection scheme by these authors [17], a

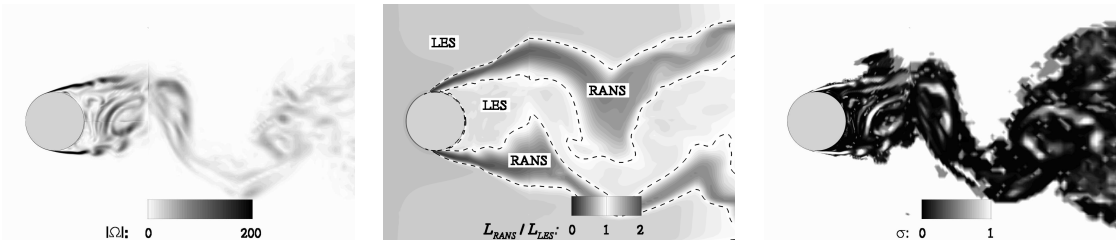


(a) Vorticity magnitude (b) LES-mode region (c) Blending function $\sigma$

*Figure 3.* Analysis of the DES and hybrid convection scheme functionality for the DES with fine time step (slice at the spanwise mid-section).

5th order upwind scheme was used, which was acknowledged as a source of significant numerical dissipation in that study.

An idea of the impact of the time step size can also be obtained from the instantaneous field. Figure 4 shows the resolution of vortical structures and the model eddy viscosity in the early shear layer for an individual snapshot for each time step size. Whereas the shear layer for the finer time step shows the development of shear layer instability, the shear layer for the coarser time step remains smooth and stable. Moreover, although the resolved turbulence is significantly reduced by the coarser time step, the level of modelled turbulence (represented by eddy viscosity ratio in Figs. 4(c) and 4(d)) remains very similar.

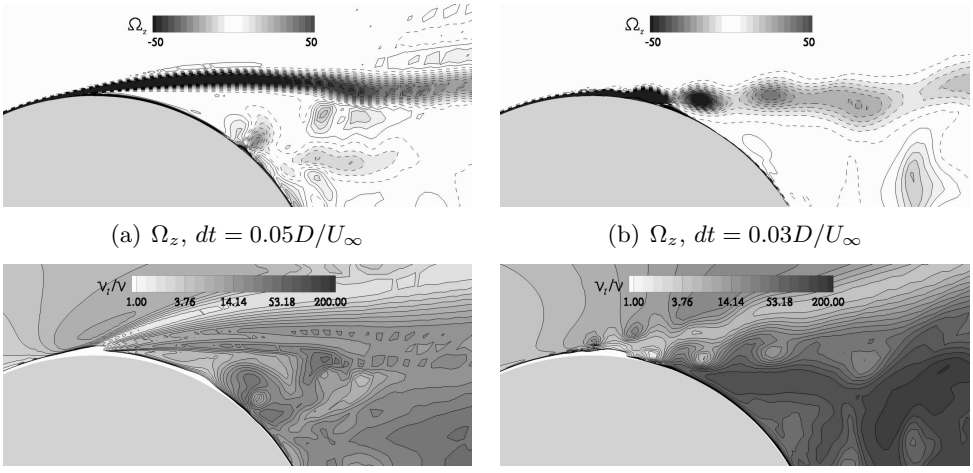


(a) $\Omega_z$, $dt = 0.05D/U_\infty$ (b) $\Omega_z$, $dt = 0.03D/U_\infty$

(c) $\nu_t/\nu$, $dt = 0.05D/U_\infty$ (d) $\nu_t/\nu$, $dt = 0.03D/U_\infty$

*Figure 4.* Effect of time filtering on resolved shear layer structures and modelled turbulence for coarse and fine time steps (contours of spanwise vorticity $\Omega_z$ and eddy viscosity ratio $\nu_t/\nu$ on a slice at the spanwise mid-section).

It appears then as if the coarser temporal resolution does not allow the formation of these structures in the shear layer, and that a form of time filtering is in effect. To obtain a rule of thumb for the balancing of spatial and temporal resolution, a

hypothetical time filter "width" can be constructed as $\Delta_t = |U| \cdot dt$. When the ratio of this to the local spatial filter width is considered, a kind of Courant-Friedrichs-Lewy (CFL) number [2] emerges:

$$\mathrm{CFL} = \frac{\Delta_t}{\Delta_x} = \frac{dt \cdot |U|}{\Delta_x}, \tag{2}$$

where $|U|$ is the local velocity magnitude and $\Delta_x$ is the DES grid length scale. The usual application of CFL numbers concerns the stability of numerical schemes, which does not apply for the implicit solver formulation used in this study. The rationale of balancing the spatial and temporal capability to resolve turbulence lies behind the selection of the quantities, hence the use of the largest grid dimension $\Delta_x$. The expectation is therefore that a criterion of CFL $\leq 1$ is necessary in all regions of resolved turbulent flow.
Figure 5 shows the distribution of the CFL number for the coarse and fine time steps. It is seen that the criterion is met throughout the domain for the finer time step, whereas values greater than unity emerge, notably at the edge of the early shear layer, for the coarser time step.

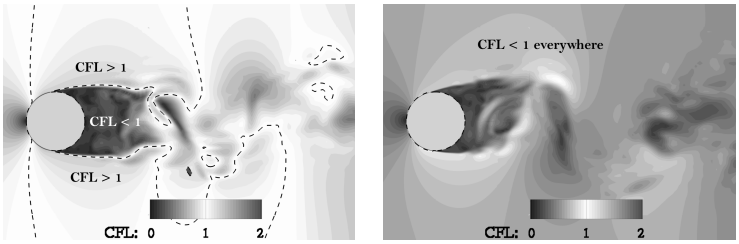


(a) CFL, $dt = 0.05D/U_\infty$ (b) CFL, $dt = 0.03D/U_\infty$

*Figure 5.* Extent of time filtering of resolved scales depicted using a CFL number for the coarse and fine time steps (slice at the spanwise mid-section).

From these observations, it seems as if this kind of CFL criterion could indeed offer a sound basis for the judgement of the sufficiency of the time step size for DES. A quantitative assessment of the time step influence will be obtained on the basis of a comparison of the time-averaged and phase-averaged flow with experimental results in the next section.

### 4.2. Time-averaged flow field

The entire numerical domain was time-averaged following the establishement of a fully-developed flow state and the elimination of initial transient artefacts. As the region within one diameter of each side wall was observed to be essentially homogeneous in the spanwise direction [11], additional averaging was then conducted along this direction.

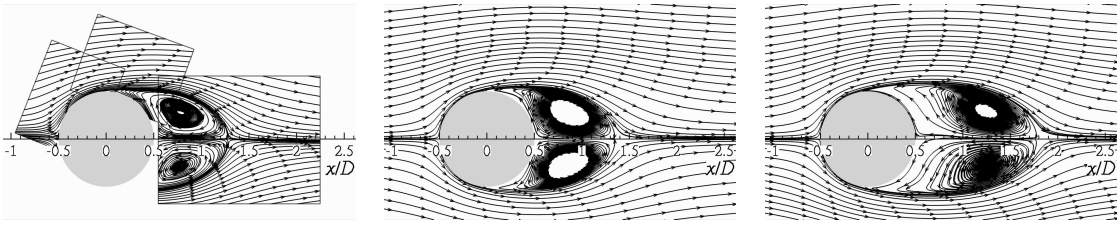


(a) PIV (b) DES, $dt = 0.03D/U_\infty$ (c) DES, $dt = 0.05D/U_\infty$

*Figure 6.* Comparison of the time-averaged streamlines for the two time steps and experiment.

Figure 6 presents a comparison of the time-averaged streamlines between the DES simulations and the experiment. It can be seen that the finer time step shows an excellent agreement, whereas the coarser time step exhibits an excessive recirculation length. The recirculation lengths (measured from the rear surface of the cylinder at $x/D = 0.5$) of the experiment, fine and coarse time step simulations are 0.78, 0.85 and 1.3 and the time-averaged pressure drag coefficient obtained at the centre plane was found to be 1.45, 1.48 and 1.32 respectively. It is interesting to note that all of the simulations presented by Travin et al. [16] suffered from an excessive recirculation length, suggesting (at least for the higher $Re$ values) that insufficient time resolution may have been a contributory factor.

The Reynolds-averaged turbulent stresses are depicted in Fig. 7 for the finer time step simulation in comparison with 2C and 3C PIV. The qualitative and quantitative agreement of the $\overline{u'u'}$ stress is excellent, whereas the effect of the mildly excessive recirculation length can be seen for the $\overline{v'v'}$ and $\overline{w'w'}$ components. Furthermore, the peak levels of $\overline{v'v'}$ are slightly over-predicted, whereas those of $\overline{w'w'}$ are slightly under-predicted.

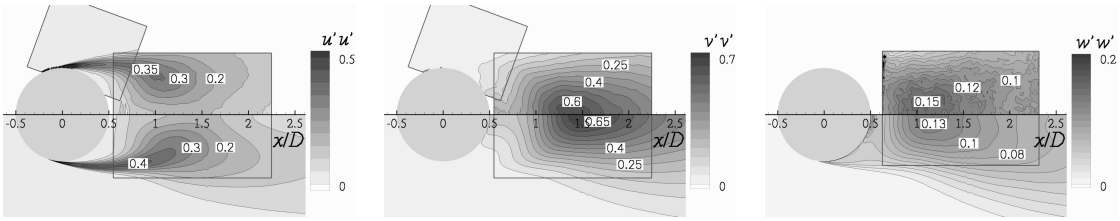


(a) $\overline{u'u'}$ (b) $\overline{v'v'}$ (c) $\overline{w'w'}$

*Figure 7.* Comparison of the resolved turbulent stress components from the fine time step DES *below* with PIV data *above*.

### 4.3. Spectral content

Velocity time traces have been extracted from the TRPIV measurements for a range of positions in the near wake shown in Fig. 8(a). Figures 8(b) and 8(c) compare the spectra obtained for the $u$ and $v$ velocity components at location 5, situated in

the time-averaged position of the shear layer at $x/D = 1$, $y/D = 0.5$. The agreement seen is generally excellent, although some significant deviations occur. The peak in the spectra represents the quasi-periodic vortex shedding, occurring at a Strouhal number of $St = 0.21$ in the experiment, and being slightly overpredicted at $St = 0.23$ by the finer time step DES (and $St = 0.245$ for the coarser time step). A fairly sharp drop off is seen at the higher frequencies, after around $St \approx 20$, which is due to either the spatial or temporal filtering of the simulation. The simulation time step corresponds to $St \approx 30$, which when combined with the Nyquist criterion results in a temporal cut-off at $St \approx 15$. It is therefore supposed that the time step, rather than the spatial resolution is responsible for this behaviour.

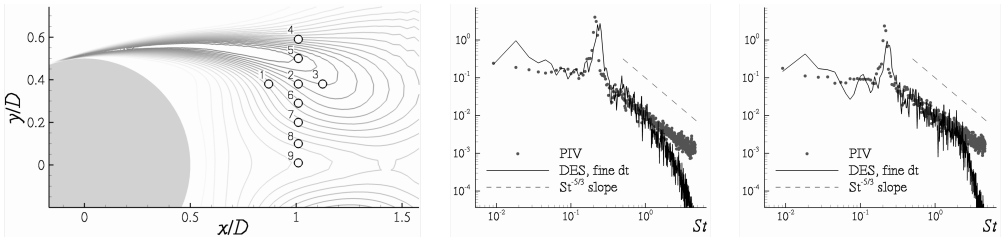


(a) Measurement positions (b) $u$-velocity, point 5 (c) $v$-velocity, point 5

*Figure 8.* Measurement positions in relationship to $\overline{u'u'}$ contours and spectra of $u$ and $v$ from the finer time step DES compared to TRPIV measurements.

### 4.4. Phase-averaged flow field

The quasi-periodic nature of the vortex shedding enables an analysis using phase-averaging to separate the coherent vortex shedding from the incoherent turbulent motions. This has been performed for both the PIV and simulation data, using the surface pressure on the cylinder as a trigger signal [8, 11], giving a further means of analysis of the unsteady prediction. Figure 9 shows the phase-averaged spanwise vorticity for the phase angle $\varphi = 45°$ for both simulations and the PIV data. The position of the shed vortices is predicted very well by the finer time step, whereas the roll-up of the shear layer can be seen to be significantly delayed for the coarser time step, resulting in a downstream displacement of the vortex locations.

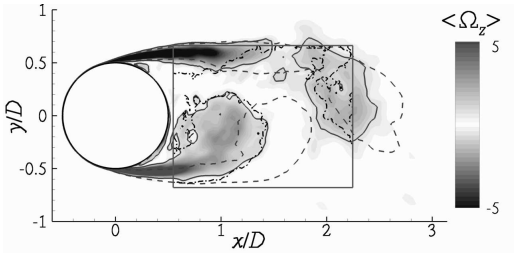


*Figure 9.* Phase-averaged spanwise vorticity $\langle\Omega_z\rangle$ for a single phase angle $\varphi = 45°$. Contour shading from DES with finer time step. Lines depict values of $\langle\Omega_z\rangle = \pm 1$ for the PIV ($- \cdot -$), DES with finer time step (—) and coarser time step ($- - -$).

## 5. Conclusion and outlook

A detailed validation of the DES implementation for the turbulent flow around a circular cylinder has been conducted, with impressive levels of agreement achieved with experimental PIV data for both time-averaged and unsteady quantities. The influence of the numerical time step has however been shown to be strong and detrimental in the case of an excessively coarse time step, giving rise to exaggerated recirculation length, reduced drag coefficient and overprediction of the vortex shedding frequency. It could be supposed that the remaining small deviations from the experimental data seen for the finer time step are a result of remaining time-filtering effects, an argument reinforced by the suggestion that temporal rather than spatial filtering determines the spectral cut-off. In order to clarify this issue, as well as to investigate the existence of an asymptotic convergence, a still finer time step should be computed. Furthermore, analysis based on the coarse time step simulation would be more rigourous by further computation in time. In the interests of obtaining concrete best-practice guidelines for the selection of the time step, the relevance of the CFL parameter has been investigated. Although giving values below unity for the finer time step, the fact that residual time filtering effects are suspected suggests that this is too conservative. The consideration of Nyquist arguments might indeed imply that the target CFL $\leq 0.5$ is more appropriate. Having established the time step dependency, the exploration of model modifications targeted at reducing this would be of considerable use in practical applications of DES.

## Acknowledgements

The authors gratefully acknowledge the support of this work in the framework of the DESider project. DESider (Detached-Eddy Simulation for Industrial Aerodynamics) is funded by the European Community represented by the CEC, Research Directorate-General, in the 6th Framework Program, under Contract No. AST3-CT-2003-502842.
The computations were conducted on the IBM pSeries 690 at the Zuse-Institut Berlin (ZIB), part of the Norddeutschen Verbund für Hoch- und Höchstleistungsrechnen (HLRN).

## References

[1] U. Bunge, C. Mockett, and F. Thiele. Guidelines for implementing detached-eddy simulation using different models. *Aerospace Science and Technology*, 2007. To be published.

[2] R. Courant, K. Friedrichs, and H. Lewy. Über die partiellen Differenzengleichungen der mathematischen Physik. *Mathematische Annalen*, 100(1):32–74, 1928.

[3] W. Haase, B. Aupoix, U. Bunge, and D. Schwamborn, editors. *FLOMANIA - A European initiative on flow physics modelling*, volume 94 of *Notes on Numerical Fluid Mechanics and Multidisciplinary Design*. Springer Verlag, 2006.

[4] F. Lien and M. Leschziner. Computational modelling of 3D turbulent flow in S-diffuser and transition ducts. In W. Rodi and F. Martelli, editors, *Engineering Turbulence Modelling and Experiments 2*, pages 217–228. Elsevier, 1993.

[5] H. Lübcke, T. Rung, and F. Thiele. Prediction of the spreading mechanisms of 3D turbulent wall jets with explicit Reynolds-stress closures. In W. Rodi and N. Fueyo, editors, *Engineering Turbulence Modelling and Experiments 5*, pages 127–145. Elsevier, 2002.

[6] F. Menter and M. Kuntz. *The Aerodynamics of Heavy Vehicles: Trucks, Buses, and Trains*, volume 19 of *Lecture notes in applied and computational mechanics*, chapter Adaption of eddy-viscosity turbulence models to unsteady separated flow behind vehicles. Springer Verlag, 2004.

[7] C. Mockett, U. Bunge, and F. Thiele. Turbulence modelling in application to the vortex shedding of stalled airfoils. In W. Rodi and M. Mulas, editors, *Engineering Turbulence Modelling and Experiments 6*, pages 617–626. Elsevier, 2005.

[8] R. Perrin. *Analyse physique et modélisation d'ecoulements incompressibles instationnaire turbulents autor d'un cylindre circulaire à grand nombre de Reynolds.* PhD thesis, Institut National Polytechnique de Toulouse, 5th July 2005.

[9] R. Perrin, M. Braza, E. Cid, S. Cazin, A. Barthet, A. Sevrain, C. Mockett, and F. Thiele. Phase averaged turbulence properties in the near wake of a circular cylinder at high Reynolds number using POD. In *Proceedings of the 13th International Symposium on Applications of Laser Techniques to Fluid Mechanics*, Lisbon, Portugal, 2006.

[10] R. Perrin, M. Braza, E. Cid, S. Cazin, P. Chassaing, C. Mockett, T. Reimann, and F. Thiele. Coherent and turbulent process analysis in the flow past a circular cylinder at high Reynolds number. In *Proceedings of the IUTAM Symposium on Unsteady Separated Flows and their Control*, Corfu, Greece, June 18–22 2007. To be published.

[11] R. Perrin, C. Mockett, M. Braza, E. Cid, S. Cazin, A. Sevrain, P. Chassaing, and F. Thiele. Joint numerical and experimental investigation of the flow around a circular cylinder at high Reynolds number. In *PIVNET 2*. 2007. To be published.

[12] C. Rhie and W. Chow. Numerical study of the turbulent flow past an airfoil with trailing edge separation. *AIAA Journal*, 21:1325–1332, 1983.

[13] P. Spalart. Young person's guide to detached-eddy simulation grids. NASA contractor report NASA/CR-2001-211032, 2001.

[14] P. Spalart, S. Deck, M. Shur, K. Squires, M. Strelets, and A. Travin. A new version of detached-eddy simulation, resistant to ambiguous grid densities. *Theoretical and Computational Fluid Dynamics*, 20:181–195, 2006.

[15] P. Spalart, W. Jou, M. Strelets, and S. Allmaras. Comments on the feasibility of LES for wings, and on a hybrid RANS/LES approach. *Advances in DNS/LES*, 1, 1997.

[16] A. Travin, M. Shur, M. Strelets, and P. Spalart. Detached-eddy simulations past a circular cylinder. *Flow, Turbulence and Combustion*, 63(1):293–313, 2000.

[17] A. Travin, M. Shur, M. Strelets, and P. Spalart. Physical and numerical upgrades in the detached-eddy simulation of complex turbulent flows. In *Proceedings of the 412th Euromech Colloquium on LES and Complex Transitional and Turbulent Flows*, Munich, Germany, 2000.

[18] L. Xue. *Entwicklung eines effizienten parallelen Lösungsalgorithmus zur dreidimensionalen Simulation komplexer turbulenter Strömungen.* PhD thesis, Technische Universität Berlin, Universitätsbibliothek (Diss.-Stelle), 1998.